Dalton Transactions

Fine control on the photochemical and photobiological properties of Ru(II) arene complexes

Journal:	*Dalton Transactions*
Manuscript ID:	DT-ART-03-2015-000939.R1
Article Type:	Paper
Date Submitted by the Author:	10-Mar-2015
Complete List of Authors:	Chen, Yong-Jie; technical institute of physical chemistry, Lei, Wan-Hua Hou, Yuan-Jun li, chao; technical institute of physical chemistry, Jiang, Guo-yu; technical institute of physical chemistry, Zhang, Bao-Wen Zhou, Qian-Xiong Wang, Xuesong; Technical Institute of Physics and Chemistry,CAS ,

Cite this: DOI: 10.1039/c0xx00000x

www.rsc.org/xxxxxx

ARTICLE TYPE

Fine control on the photochemical and photobiological properties of Ru(II) arene complexes

Yongjie Chen[a, b], Wanhua Lei[a] , Yuanjun Hou[a], Chao Li[a], Guoyu Jiang[a], Baowen Zhang[a], Qianxiong Zhou*[a], Xuesong Wang*[a]

Received (in XXX, XXX) Xth XXXXXXXXX 20XX, Accepted Xth XXXXXXXXX 20XX
DOI: 10.1039/b000000x

A series of six Ru(arene) complexes, $[(\eta^6\text{-}p\text{-cymene})Ru(dpb)(py\text{-}R)]^{2+}$ (**1-6**, dpb = 2,3-bis(2-pyridyl)benzoquinoxaline, py-R = 4-substituted pyridine, R = $N(CH_3)_2$, NH_2, OCH_3, H, $COOCH_3$ and NO_2), were synthesized and their photochemical and photobiological properties were compared in detail. The electron push/pull character of the R groups has a significant impact on both ligand photodissociation and $^1O_2$ generation of the complexes. The photoinduced DNA covalent binding capabilities increase from **1** to **6** in both aerobic and anaerobic conditions, and DNA photocleavage occurs simultaneously in aerobic environments. **4** has the most potent phototoxicity against human lung carcinoma A549 cells among the examined complexes. The substituent effect may ascribed to the influences of the R groups on the energy levels of ^{3}MC and ^{3}MLCT states as well as the energy gaps between ^{3}MC, ^{3}MLCT and dpb-based ^{3}IL states. Similar chemical modification on bidentate and arene ligands or other sites of the pyridine ligand may lead to more efficient agents with PDT and/or PACT activities.

Introduction

Photodynamic therapy (PDT) and photoactivated chemotherapy (PACT) are two cancer treatment modalities that need activation by light of proper wavelengths. With respect to regular chemotherapy, the spatially and temporally controlled illumination endows both methods higher selectivity and specificity against tumor cells and lower side effects toward normal cells.[1] While sharing this common benefit, PDT and PACT have their own merits and limits. PDT utilizes reactive oxygen species (ROS), mainly singlet oxygen ($^1O_2$), to eradicate tumor cells. $^1O_2$ is generated by energy transfer from the excited photosensitizer molecules to oxygen,[2] a process proceeds catalytically, *i.e.* one photosensitizer molecule can generate many $^1O_2$ molecules, partly accounting for the high efficiency of PDT. However, the oxygen-dependant character of PDT limits its efficacy toward hypoxic tumor cells.[3] While both organic chromophores[4] and transition metal complexes[5] have been examined for PDT application, the PACT agents developed so far are mainly transition metal complexes.[6] They have low cytotoxcity in the dark but undergo ligand dissociation upon irradiation and then covalent binding to DNA or other cellular components in a manner similar to cisplatin.[7] Though PACT can work in both aerobic and anaerobic conditions, it generates cytotoxic species stoichiometrically, rather than catalytically like its PDT counterpart. A higher anticancer efficacy and a broader anticancer spectrum may be achieved simultaneously by fusing PACT and PDT in one agent. Up to now, a variety of transition metal complexes are proven to be either PDT or PACT active,[6, 8-12] however, examples that possess dual potentials of PDT and PACT are rare and mainly belong to bimetal complexes with one nuclear having PDT activity and the other showing PACT function.[13] In our continuous effort to develop Ru-based PACT agents with long photoactivation wavelength, we synthesized and scrutinized an intriguing mononuclear Ru(II) arene complex, $[(\eta^6\text{-}p\text{-cymene})Ru(dpb)(py)]^{2+}$ (dpb = 2,3-bis(2-pyridyl)benzoquinoxaline, py = pyridine, complex **4** in Scheme 1). The highly delocalized nature of dpb makes its long lived triplet excited state (^{3}dpb*) the lowest-lying excited state of the complex, rendering the complex $^1O_2$ generation and DNA photocleavage ability.[14] Additionally, the bulky feature of dpb forces the complex to adopt a distorted octahedral geometry and allows for dissociation of not only py but also dpb upon irradiation, endowing the complex with efficient DNA photobinding capability.[14] Very recently, C. Turro, K. R. Dunbar and coworkers also found dual action of $^1O_2$ and ligand dissociation in a new tris-heteroleptic complex $[Ru(bpy)(dppn)(CH_3CN)_2]^{2+}$ (bpy = 2,2′-bipyridine, dppn = benzo[i]dipyrido[3,2-a;2′,3′-c]phenazine).[15] The promising properties of $[(\eta^6\text{-}p\text{-cymene})Ru(dpb)(py)]^{2+}$ encouraged us to further explore its structure-activity relationship with the aim to develop more efficient metallodrugs with both PDT and PACT activities. In this work, a series of $[(\eta^6\text{-}p\text{-cymene})Ru(dpb)(py\text{-}R)]^{2+}$ complexes (py-R = 4-substituted pyridine, Scheme 1) were synthesized and their photochemical and photobiological properties were compared to disclose the substituent effect on the py ligand. The substituent R covers a wide range of electron push-pull characters, from electron-donating groups of $N(CH_3)_2$, NH_2, and OCH_3 to electron-withdrawing groups of $COOCH_3$ and NO_2. It was found that the electron-withdrawing groups facilitate both $^1O_2$

generation and ligand dissociation. The manner of ligand dissociation, *i.e.* py or dpb dissociation, is also highly dependent on the chemical identity of the R group. The underlying mechanism is discussed, which may assist in rationale design of new Ru complexes with PDT and/or PACT activities.

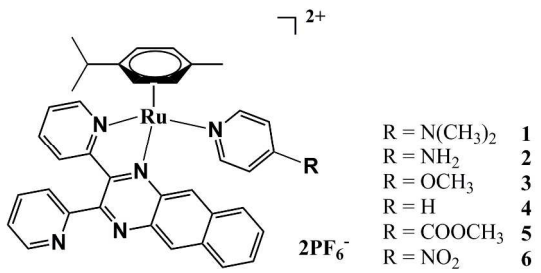

Scheme 1 Chemical structures of the examined Ru(II) arene complexes.

Results and discussion

Photophysical properties

Figure 1 shows the normalized UV-visible absorption spectra of the examined complexes in CH_3CN. Though modified by different substituent at 4-position of the pyridine ligand, **1-3** and **4-5** exhibit absorption spectra nearly identical to that of **4**. Based on our previous studies,[14] The absorption bands centered at 330 and 405 nm can be ascribed to the dpb-based ^{1}IL (intra-ligand) transitions, and the absorption tail extending beyond 600 nm may be attributed to ^{1}MLCT (metal to ligand charge transfer) transition from Ru-based t_{2g} orbital to dpb-based π^* orbital. With the increase of the electron donating property of the substituent, the t_{2g} orbital is expected to be destabilized and thus a red shift of ^{1}MLCT transition is anticipated. For the complexes of $[Ru(II)(tpy)(dppz)(py\text{-}R)]^{2+}$ (tpy = 2,2′:6′,2″-terpyridine, dppz = dipyrido[3,2-a:2′,3′-c]phenazine, py-R = 4-substituted pyridine; R = $N(CH_3)_2$, NH_2, OCH_3, H, NO_2), bathochromic shift of ^{1}MLCT band with the increase of the electron donating strength of R were indeed observed.[16] The lack of ^{1}MLCT shift among **1-6** is likely

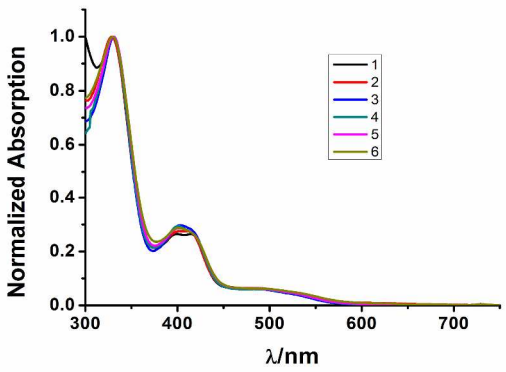

Fig. 1 Normalized absorption spectra of **1-6** in CH_3CN.

due to somewhat superposition between the strong dpb-based ^{1}IL transition and the weak ^{1}MLCT transition, which leads to no observation of ^{1}MLCT maxima and therefore their shift along with the variation of the R group. The fact that 405 nm band rather than 330 nm band underwent slight changes from **1** to **6** seems in good agreement with our assumption.

While the free dpb ligand is fluorescent, all the examined complexes are non-luminescent, a general behavior of Ru(II) arene complexes.[17] The fluorescence quenching of dpb upon coordination suggests an efficient transition from ^{1}dpb* to ^{1}MLCT. Based on the absorption and emission properties, it is expected that the ^{1}MLCT state of **1-6** is in close proximity to but slightly lower than dpb-based ^{1}IL state in energy.

Photoinduced ligand dissociation

Before examining the photoinduced ligand dissociation, we at first evaluated the stability of **1-6** in PBS buffer in the dark (Figure S1-S6, ESI). Similar to **4**, no discernible changes in UV-visible absorption spectra were observed for the solutions of **1-3** after standing for 4 h, demonstrating their satisfactory stability. In contrast, the PBS solutions of **5** and **6** underwent a little bit changes, meanwhile the solutions remained non-luminescent, suggesting the dissociation of py-R (R = $COOCH_3$ and NO_2). Obviously, the tethering of electron-withdrawing group on pyridine diminishes its coordination ability and makes it somewhat labile in the dark.

Upon irradiation (λ > 470 nm), all the PBS solutions of **1-6** experienced remarkable changes in both UV-visible absorption and emission spectra, as shown in Figure S7-S12 (ESI). Our previous studies have shown that **4** will release either pyridine or dpb upon irradiation in PBS, and the dissociation of dpb from the complex leads to partial fluorescence restoration.[14] Clearly, **1-3** and **5-6** undergo photoinduced ligand dissociation, just like their parent complex **4**. Based on the extents of fluorescence recovery, the photoinduced dissociation rates of dpb may be roughly estimated to follow the order of **4** > **3** > **2** > **5** > **1** > **6**. Due to spectrum overlap among the original complex and both types of ligand-dissociation products, it is difficult to compare the dissociation rates of py-R from UV-visible spectra. This issue may be fully addressed by ^{1}H NMR measurements.

Table 1. Monodentate ($\eta_{py\text{-}R}$) and bidentate (η_{dpb}) ligand dissociation yields of **1-6** in CD_3COCD_3:D_2O (1:2) after irradiation (λ > 400 nm) for 12 h.

	1	**2**	**3**	**4**	**5**	**6**
$\eta_{py\text{-}R}$	--	--	21%	37%	59%	68%
η_{dpb}	--	--	8%	12%	7%	--

Based on ^{1}H NMR data; -- represents negligible.

The chemical shifts of the two protons (H_a and H_b) of dpb in the central ring of benzoquinoxaline can be discriminated with each other among the free dpb, the original complex, and the py-leaving product.[14] Taking advantage of this property, the photoinduced ligand dissociation behaviors of **1-6** were compared as shown in Figure 2 and S13-14 (ESI), and total ligand dissociation proportions as well as monodentate and bidentate ligand dissociation proportions are collected in Table 1. From **1** to **6**, the monodentate ligand dissociation rates increased gradually, in line with the coordination ability of py-R. In contrast, the most efficient dpb dissociation occurred in **4**. Modification by either electron-donating or electron withdrawing group on py results in a decrease in the dpb dissociation. This

result is largely in line with the trends of fluorescence restoration in PBS solutions. It is worth noting that the photodissociation rates of **1-6** in CD_3COCD_3:D_2O and other organic solvents (*e.g.* CH_3CN) are significantly lowers than in PBS. Similar phenomena were also found in our previous studies.[14]

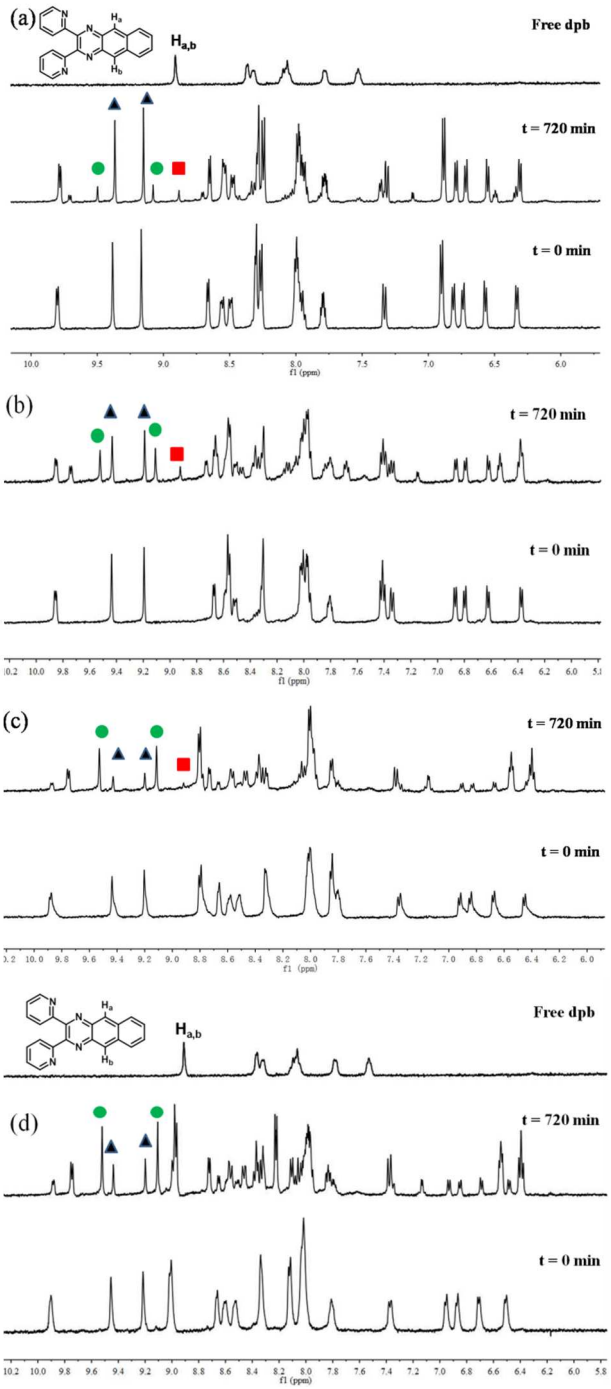

Fig. 2 ^{1}H NMR spectra of **3** (a), **4** (b), **5** (c) and **6** (d) in CD_3COCD_3:D_2O (1:2) before and after irradiation (λ > 400 nm) for 12 h. The chemical shifts of the two protons (H_a and H_b) on the central ring of benzoquinoxaline in the original complex, the py-R-leaving product and the free dpb are labeled by ▲, ● and ■, respectively.

$^1O_2$ generation

The most interesting property of **4** lies in its $^1O_2$ generation ability, which in turn is the result of the long lived dpb-based ^{3}IL state becoming the lowest lying triplet excited state of the complex.[14] In this work, we at first qualitatively compared the $^1O_2$ generation by **1-6** using EPR spin trapping technique. As shown in Figure S15 (ESI), upon irradiation (by a 532 nm laser) of oxygen-saturated CH_3CN solutions of the examined Ru complexes and TEMP, three-line signals with a hyperfine coupling constant of 16.0 G, in good agreement with TEMPO (the adduct of TEMP and $^1O_2$),[18] were observed. Control experiments indicate that both irradiation and oxygen are necessary for the formation of the signals. Additionally, NaN_3, a common scavenger of $^1O_2$, can quench the signal effectively, vindicating the $^1O_2$ origin of the signals further. When the absorbance of the irradiated samples at 532 nm was adjusted to the same, we obtained a sequence of **6** > **5** > **4** > **3** > **2** ≈ **1** in $^1O_2$ generation based on the TEMPO signal intensities (Figure 3).

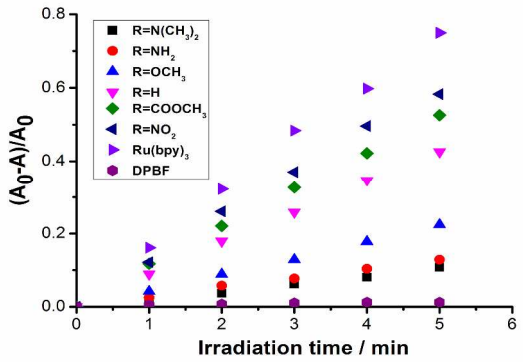

Fig. 3 EPR signals obtained upon irradiation of O_2-saturated CH_3CN solutions of 50 mM TEMP and 0.8-1.0 mM Ru complexes for 30 s with a 532 nm laser (the absorbance at 532 nm was kept constant).

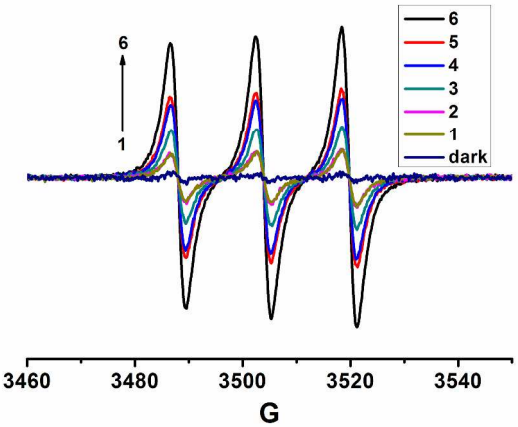

Fig. 4 DPBF bleaching (at 405 nm) in the presence of **1-6** in CH_3CN upon irradiation at 500 nm.

We then compared the $^1O_2$ generation abilities of **1-6** in a more quantitative manner. DPBF can react efficiently with $^1O_2$ to form an endoperoxide product, a process that can be easily followed by monitoring the bleaching of DPBF.[19] Using DPBF as the chemical trapping agent of $^1O_2$ and $[Ru(bpy)_3]^{2+}$ as a reference

(Φ_Δ = 0.57 in CH_3CN[20]), the $^1O_2$ quantum yields were measured to be 0.07 for **1**, 0.09 for **2**, 0.15 for **3**, 0.25 for **4**, 0.34 for **5** and 0.39 for **6** (Figure 3 and Table 2), in good agreement with the EPR results. Under the same irradiation condition, no detectable ligand photodissociation was observed (Figure S16, ESI), indicating that $^1O_2$ originates from **1-6** themselves.

Table 2 $^1O_2$ quantum yields and triplet excited state lifetimes of **1-6**.

	1	**2**	**3**	**4**	**5**	**6**
$\tau^{[a]}$/μs	0.06	0.5	1.3	1.9	1.9	2.0
$^1O_2$ quantum yields[b]	0.07	0.09	0.15	0.25	0.34	0.39

[a] In Ar-saturated CH_3CN, [b] in air-saturated CH_3CN.

To better understand the different $^1O_2$ generation capabilities of the examined complexes, we further measured their transient absorption spectra in Ar-saturated CH_3CN. Basically, **1-3** and **5-6** exhibit T-T absorption spectra very similar to that of **4** (Figure 5), which has been ascribed to dpb-based ^{3}IL state in our previous work.[14] Figure S17 shows the T-T absorption of the free dpb ligand. The spectra difference beyond 550 nm between the free dpb ligand and **4** was ascribed to the emission of the free dpb ligand in our previous publication.[14] However, the fluorescence of the free dpb ligand cannot extend beyond 700 nm. Further, the fluorescence lifetime should be in the ns region. As a result, a more reasonable explanation may be as follows. Due to proximity in energy between the ^{3}MLCT and ^{3}dpb* states, the ^{3}MLCT state may be populated simultaneously along with the ^{3}dpb* state, and the observed spectra should originate from the mixing of ^{3}dpb* and ^{3}MLCT states. The fact that $[Ru(bpy)_2(dpb)]^{2+}$ showed strong absorption beyond 600 nm in its T-T absorption spectra[5c] supports this explanation (Figure S18). The lifetimes undergo a gradual increase from 0.06 μs for **1** to 2.0 μs for **6**, accounting for the gradual enhancement from **1** to **6** in $^1O_2$ generation.

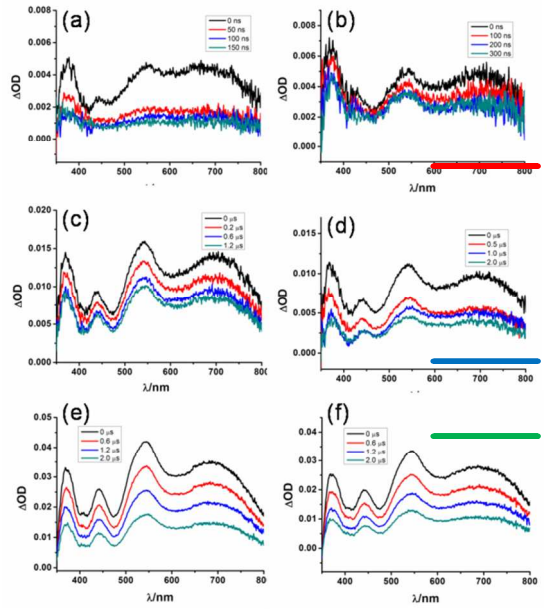

Fig. 5 Transient absorption spectra of **1-6** (a-f) in Ar-saturated CH_3CN solutions upon pulsed excitation at 400 nm.

We also determined the $^1O_2$ generation by **1-6** in PBS in which photoinduced ligand dissociation took place far efficiently than in CH_3CN. As shown in Figure S19 (ESI), a new order of **4** > **5** > **3** > **6** ≈ **2** ≈ **1** was observed. **4** becomes the most active one in $^1O_2$ generation in PBS. The result may be attributed to the much improved ligand dissociation of **5** and **6** in PBS (Table 1).

Mechanism behind the substituent effect

The effects of the R substituents on the photoinduced ligand dissociation and $^1O_2$ generation of **1-6** may be rationalized by taking into account the energy gap changes between ^{3}MC, dpb-based ^{3}MLCT and dpb-based ^{3}IL. The three triplet excited states should follow the order ^{3}MC > ^{3}MLCT > ^{3}IL in energy. Moreover, the energy gaps between them are anticipated to be small enough to allow for thermal activation from ^{3}MLCT to ^{3}MC and from ^{3}IL to ^{3}MLCT. The photoinduced ligand dissociation behaviors of **1-6**, a process that generally occurs in ^{3}MC via thermal activation from ^{3}MLCT, are in line with the former assumption, while the close proximity in energy between dpb-based ^{1}IL and ^{1}MLCT (*vide supra*) seems in line with the later one. Because modification is on the monodentate ligand, the dpb-based ^{3}IL may be assumed to remain unchanged throughout **1-6**. Thus, as shown in Scheme 2, the presence of electron-withdrawing group will, on one hand, stabilize Ru-based t_{2g} orbital and thus lift the energy level of ^{3}MLCT. On the other hand, the weakened ligand field leads to a reduction of ^{3}MC in energy. As a result, energy gap between ^{3}MC and ^{3}MLCT is narrowed, favoring ligand dissociation from ^{3}MC. Meanwhile, the energy gap between ^{3}MLCT and ^{3}IL is enlarged, inhibiting deactivation of ^{3}IL through ^{3}MLCT, a state generally shows shorter lifetime than purely organic counterpart, favoring $^1O_2$ generation from ^{3}IL. Opposite effects are expected in the cases of **1-3**. By way of simple control of the electron push/pull character of the substituent on pyridine, the ligand dissociation and $^1O_2$ generation of **1-6** are finely tuned. The more efficient ligand photodissociation in purely aqueous solutions than in organic solutions might be due to the larger polarity of water, which will stabilize the ^{3}MC (with Ru-σ^*(L) character) and ^{3}MLCT states, both are charge transfer states in nature, and therefore favour their

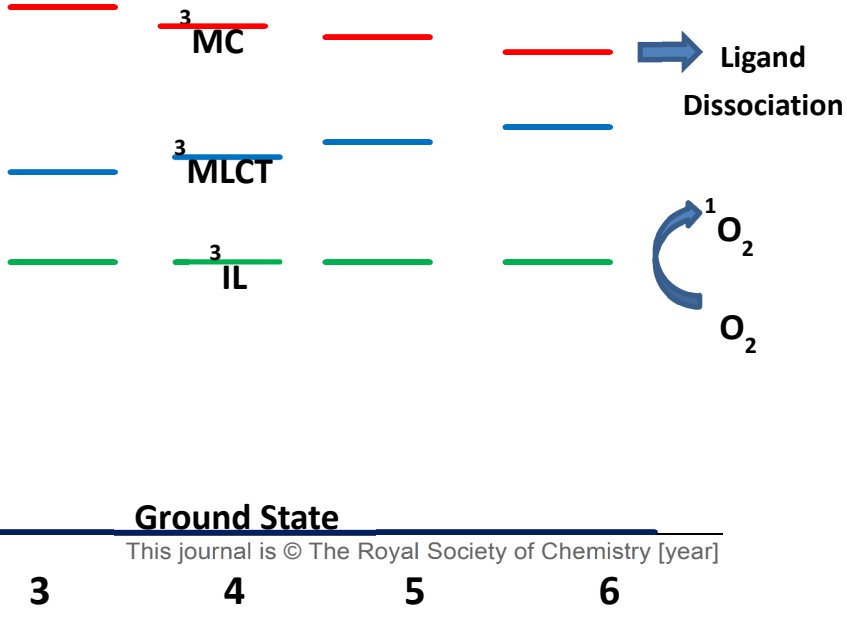

population from the lowest-lying ^{3}dpb* state, whose energy level is expected to be affected by solvents less significantly than those of the ^{3}MC and ^{3}MLCT states.

Scheme 2 Schematic representation of the effect of the substituent on pyridine on the triplet excited state energy levels of **1-6**.

DNA covalent binding and cleavage

The photoinduced DNA damage abilities of **1-6** in different conditions were compared by agarose gel electrophoresis using supercoiled pUC19 DNA as the target. In Ar-saturated PBS solutions, **1-6** cannot generate $^1O_2$ but may only undergo ligand dissociation. The resultant Ru(arene) fractions may then covalently bind to DNA, resulting in the retardation of DNA mobility. This is what we observed as shown in Figure 6b. Notably, the retardation extents accord very well with the order of the ligand dissociation rates, *i.e.* **6** > **5** > **4** > **3** > **2** > **1**. Additionally, covalent binding also led to significant bleaching of the supercoiled circular (SC) band since EB intercalation and staining was restricted.

In contrast, in air-saturated conditions, nicked circular (NC) bands were observed (Figure 6a), indicating $^1O_2$ generation and SC cleavage. Because the ligand dissociation products underwent covalent binding also toward NC form, which led to retardation and bleaching of the NC band, the fluorescence intensity of the NC band had no linear correlation with the $^1O_2$ generation abilities of **1-6**.

We also examined the DNA damage particularly by **5** and **6** in the dark since both of them are not as stable as **1-4** (*vide supra*). As shown in Figure S20 (ESI), all the examined complexes including **5** and **6** neither covalently bound nor cleaved DNA in our experimental conditions, consistent with negligible absorption and emission spectra changes of **1-6** due to short incubation time (only 2 h), and indicating the DNA covalent binding and cleavage observed in Figure 6 are photoactivated.

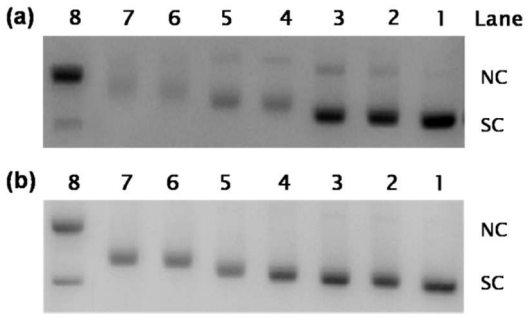

Fig. 6 Agarose gel electrophoresis pattern of supercoiled pUC19 DNA (40 μg mL^{-1}) in air-saturated (a) and Ar-saturated (b) PBS (pH = 7.4) irradiated at λ > 470 nm for 40 min in the presence of 80 μM Ru complexes. Lane 1, supercoiled DNA alone; lane 2, DNA + **1**; lane 3, DNA + **2** ; lane 4, DNA + **3**; lane 5, DNA + **4**; lane 6, DNA + **5**; lane 7, DNA + **6**; lane 8, nicked circular DNA (obtained by irradiation in the presence of $[Ru(bpy)_3]^{2+}$).

Cytotoxicity

Our previous studies showed that **4** had significant light-enhanced cytotoxicity toward human lung carcinoma cells A549. In this work, the cytotoxic activities of **1-3** and **5-6** against A549 cells were compared with that of **4** under both dark and irradiation (> 400 nm) conditions. Cells were incubated with Ru-complexes for 4 h in the dark before irradiation for 1 h, then incubated for another 20 h in the dark. Dark controls were run in parallel. Cell survival was quantified by way of an MTT assay.

As shown in Figure 7 and Table S1 (ESI), no light-enhanced cytotoxicity was observed for **1** and **2**, in line with their lower ligand photodissociation and $^1O_2$ generation efficiencies. In the cases of **3-6**, photocytotoxicity can be detectable. Among them, **4** seems the most active one. For example, at 10 μM and under irradiation, the cell survival was only 16% for **4**, but 45%, 34% and 50% for **3**, **5** and **6**, respectively. The most potent phototoxicity of **4** might be associated to its highest activity in $^1O_2$ generation in PBS. Considering the fact that the ligand photodissociation rates are highly dependent on the microenvironment that the complexes exist in, the contribution of the ligand photodissociation is still unclear.

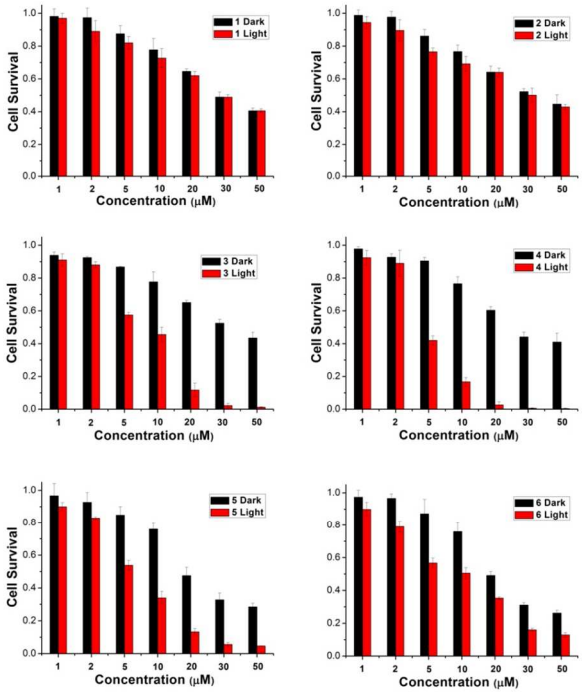

Fig. 7 Cytotoxicities of **1-6** against A549 cells in the dark or under irradiation (λ > 400 nm) for 1 h.

Conclusion

By tethering a substituent with varied electron push/pull strengths at the 4-postion of pyridine, we realized fine tune on the photoinduced ligand dissociation and $^1O_2$ generation of $[(\eta^6$-*p*-cymene) Ru(dpb)(py-R)$]^{2+}$ and their DNA photobinding and photocleavage capabilities. The underlying mechanism may be ascribed to the influences of the R groups on the energy levels of ^{3}MC and ^{3}MLCT as well as the energy gaps between ^{3}MC, ^{3}MLCT and dpb-based ^{3}IL. Similar modification at different sites of the pyridine ligand or at bidentate and arene ligands may lead to more efficient agents with PDT and/or PACT activities.

Experimental section

Materials

4-Dimethylaminopyridine, 4-aminopyridine, 4-methoxypyridine, pyridine, methyl isonicotinate, 4-nitropyridine, [(*p*-cymene)$RuCl_2$]$_2$, NH_4PF_6, $AgNO_3$, 1,3-diphenylisobenzofuran (DPBF), 9,10-anthracenediyl-bis(methylene) dimalonic acid (AMDA), sodium azide (NaN_3), 2,2,6,6-tetramethyl-4-piperidone (TEMP), gel loading buffer, tris-hydroxymethyl-aminomethane (Tris base), ethidium bromide (EB), tetra-*n*-butylammonium hexafluorophosphate and ethylenediaminotetracetic acid (EDTA) were purchased from Sigma-Aldrich. Supercoiled pUC19 plasmid DNA was obtained from TaKaRaBiotechology.

Synthesis

Dpb was synthesized following the reported method.[21] The complexes **1-6** were prepared following our published method.[14] Taking **1** as an example, 122.5 mg [(*p*-cymene)$RuCl_2$]$_2$ and 133.7 mg dpb were refluxed in 10 mL methanol for 4 h. After cooling to room temperature, 10 mL of $AgNO_3$ (136 mg) aqueous solution was added. After reflux for 3 h, the reaction solution was filtered. The filtrate was then refluxed again for 4 h, with 4-dimethylaminopyridine (4 equiv) added. The whole reactions were conducted under N_2 atmosphere. After removal of solvent, the solid was purified by column chromatography on silica gel using $CH_3CN/H_2O/KNO_3$ (40:4:1) as eluent. The obtained compound was dissolved in water and precipitated by NH_4PF_6, and the orange solid was filtered, washed with water and dried under vacuum. Yield, 75%. The synthetic methods of other complexes were similar to that of **1**, using corresponding monodentate ligands.

[(η^6-*p*-cymene)Ru(dpb)(py-N(CH_3)$_2$)](PF_6)$_2$ (1). ^{1}H NMR (400 MHz, in [D_6] DMSO): δ = 0.81 (d, 3H, *J* = 6.8 Hz), 0.95 (d, 3H, *J* = 6.8 Hz), 2.20 (s, 3H), 2.37-2.43 (m, 1H), 3.86 (s, 6H), 6.43-6.47 (m, 3H), 6.52 (d, 1H, *J* = 6.0 Hz), 6.83 (d, 1H, *J* = 6.4 Hz), 6.93 (d, 1H, *J* = 6.0 Hz), 7.18 (d, 1H, *J* = 8.0 Hz), 7.69-7.75 (m, 3H), 7.89-8.06 (m, 4H), 8.25-8.31 (m, 2H), 8.50 (d, 1H, *J* = 7.2 Hz), 8.57 (d, 1H, *J* = 4.8 Hz), 8.75 (d, 1H, *J* = 7.2 Hz), 9.23 (d, 2H, *J* = 4.8 Hz), 9.76 (d, 1H, *J* = 5.6 Hz). ESI-MS (in CH_3OH): m/z = 346.1099 (M-2PF_6)$^{2+}$, 837.1843 (M-PF_6)$^+$. Anal. Calcd for $C_{39}H_{38}F_{12}N_6P_2Ru{\cdot}2H_2O$: C, 46.02; H, 4.16; N, 8.26. Found: C, 46.02; H, 4.18; N, 8.25.

[(η^6-*p*-cymene)Ru(dpb)(py-NH_2)](PF_6)$_2$ (2). ^{1}H NMR (400 MHz, in [D_6] DMSO): δ = 0.81 (d, 3H, *J* = 6.8 Hz), 0.95 (d, 3H, *J* = 6.8 Hz), 2.22 (s, 3H), 2.36-2.43 (m, 1H), 6.29 (d, 2H, *J* = 6.8 Hz), 6.36 (d, 1H, *J* = 6.4 Hz), 6.44 (d, 1H, *J* = 6.4 Hz), 6.87-6.89 (m, 3H), 7.18 (d, 1H, *J* = 7.6 Hz), 7.62 (d, 2H, *J* = 6.4 Hz), 7.68-7.72 (m, 1H), 7.87-8.03 (m, 4H), 8.24-8.30 (m, 2H), 8.50 (d, 1H, *J* = 6.8 Hz), 8.57 (d, 1H, *J* = 5.2 Hz), 8.72 (d, 1H, *J* = 7.6 Hz), 9.19 (s, 1H), 9.21 (s, 1H), 9.69 (d, 1H, *J* = 5.6 Hz). ESI-MS (in CH_3OH): m/z = 332.0943 (M-2PF_6)$^{2+}$, 809.1530 (M-PF_6)$^+$. Anal. Calcd for $C_{37}H_{34}F_{12}N_6P_2Ru{\cdot}2H_2O$: C, 44.90; H, 3.87; N, 8.49. Found: C, 44.92; H, 3.86; N, 8.48.

[(η^6-*p*-cymene)Ru(dpb)(py-OCH_3)](PF_6)$_2$ (3). ^{1}H NMR (400 MHz, in [D_6] DMSO): δ = 0.80 (d, 3H, *J* = 6.8 Hz), 0.93 (d, 3H, *J* = 6.8 Hz), 2.18 (s, 3H), 2.34-2.41 (m, 1H), 3.75 (s, 3H), 6.49 (d, 1H, *J* = 6.0 Hz), 6.57 (d, 1H, *J* = 6.0 Hz), 6.85 (d, 1H, *J* = 6.8 Hz), 6.97-7.00 (m, 3H), 7.17 (d, 1H, *J* = 8.0 Hz), 7.71 (t, 1H, *J* = 6.0 Hz), 7.90-8.02 (m, 4H), 8.20 (d, 2H, *J* = 7.2 Hz), 8.25-8.31 (m, 2H), 8.51 (d, 1H, *J* = 7.6 Hz), 8.57 (d, 1H, *J* = 4.8 Hz), 8.75 (d, 1H, *J* = 6.8 Hz), 9.24 (s, 1H), 9.26 (s, 1H), 9.79 (d, 1H, *J* = 5.6 Hz). ESI-MS (in CH_3OH): m/z = 339.5940 (M-2PF_6)$^{2+}$, 824.1526 (M-PF_6)$^+$. Anal. Calcd for $C_{38}H_{35}F_{12}N_5OP_2Ru{\cdot}2H_2O$: C, 45.43; H, 3.91; N, 6.97. Found: C, 45.42; H, 3.92; N, 6.98.

[(η^6-*p*-cymene)Ru(dpb)py](PF_6)$_2$ (4). ^{1}H NMR (400 MHz, in [D_6] DMSO): δ = 0.79 (d, 3H, *J* = 6.8 Hz), 0.93 (d, 3H, *J* = 6.8 Hz), 2.17 (s, 3H), 2.32-2.39 (m, 1H), 6.50 (d, 1H, *J* = 5.6 Hz), 6.61 (d, 1H, *J* = 5.6 Hz), 6.87 (d, 1H, *J* = 6.0 Hz), 7.03 (d, 1H, *J* = 5.6 Hz), 7.17 (d, 1H, *J* = 8.0 Hz), 7.43 (t, 2H, *J* = 6.8 Hz), 7.71 (t, 1H, *J* = 6.8 Hz), 7.91-8.01 (m, 5H), 8.26-8.31 (m, 2H), 8.46 (d, 2H, *J* = 5.2 Hz), 8.51 (d, 1H, *J* = 7.2 Hz), 8.57 (d, 1H, *J* = 4.8 Hz), 8.75 (d, 1H, *J* = 8.0 Hz), 9.24 (s, 1H), 9.28 (s, 1H), 9.80 (d, 1H, *J* = 5.6 Hz). ESI-MS (in CH_3OH): m/z = 324.5886 (M-2PF_6)$^{2+}$, 794.1427 (M-PF_6)$^+$. Anal. Calcd for $C_{37}H_{33}F_{12}N_5P_2Ru{\cdot}1.5H_2O$: C, 46.02; H, 3.76; N, 7.25. Found: C, 46.00; H, 3.77; N, 7.26.

[(η^6-*p*-cymene)Ru(dpb)(py-$COOCH_3$)](PF_6)$_2$ (5). ^{1}H NMR (400 MHz, in [D_6] DMSO): δ = 0.80 (d, 3H, *J* = 6.8 Hz), 0.93 (d, 3H, *J* = 6.8 Hz), 2.19 (s, 3H), 2.34-2.42 (m, 1H), 3.80 (s, 3H), 6.54 (d, 1H, *J* = 6.4 Hz), 6.61 (d, 1H, *J* = 6.4 Hz), 6.85 (d, 1H, *J* = 6.4 Hz), 7.04 (d, 1H, *J* = 6.0 Hz), 7.17 (d, 1H, *J* = 7.6 Hz), 7.69-7.72 (m, 1H), 7.75 (d, 2H, *J* = 6.8 Hz), 7.89-8.02 (m, 4H), 8.24-8.30 (m, 2H), 8.50-8.53 (m, 1H), 8.57 (d, 1H, *J* = 4.8 Hz), 8.66 (d, 2H, *J* = 6.8 Hz), 8.71-8.74 (m, 1H), 9.24 (s, 1H), 9.27 (s, 1H), 9.81 (d, 1H, *J* = 5.6 Hz). ESI-MS (in CH_3OH): m/z = 353.5915 (M-2PF_6)$^{2+}$, 852.1477 (M-PF_6)$^+$. Anal. Calcd for $C_{39}H_{35}F_{12}N_5O_2P_2Ru{\cdot}H_2O$: C, 46.16; H, 3.68; N, 6.90. Found: C, 46.15; H, 3.67; N, 6.92.

[(η^6-*p*-cymene)Ru(dpb)(py-NO_2)](PF_6)$_2$ (6). ^{1}H NMR (400 MHz, in [D_6] DMSO): δ = 0.79 (d, 3H, *J* = 6.8 Hz), 0.93 (d, 3H, *J* = 6.8 Hz), 2.21 (s, 3H), 2.33-2.38 (m, 1H), 6.57 (d, 1H, *J* = 6.0 Hz), 6.64 (d, 1H, *J* = 6.0 Hz), 6.87 (d, 1H, *J* = 6.4 Hz), 7.06 (d, 1H, *J* = 5.6 Hz), 7.18 (d, 1H, *J* = 8.8 Hz), 7.71 (t, 1H, *J* = 6.0 Hz), 7.92-8.03 (m, 4H), 8.08 (d, 2H, *J* = 7.2 Hz), 8.25-8.31 (m, 2H), 8.52 (d, 1H, *J* = 8.0 Hz), 8.58 (d, 1H, *J* = 4.4 Hz), 8.72 (d, 1H, *J* = 7.2 Hz), 8.82 (d, 2H, *J* = 6.8 Hz), 9.26 (d, 2H, *J* = 6.8 Hz), 9.84 (d, 1H, *J* = 5.2 Hz). ESI-MS (in CH_3OH): m/z = 347.0812 (M-2PF_6)$^{2+}$, 839.1272 (M-PF_6)$^+$. Anal. Calcd for $C_{37}H_{32}F_{12}N_6O_2P_2Ru{\cdot}2H_2O$: C, 43.58; H, 3.56; N, 8.24. Found: C, 43.60; H, 3.57; N, 8.22.

Spectroscopic measurements

^{1}H NMR spectra were recorded on a Bruker DMX-400 MHz spectrophotometer, using $SiMe_4$ as standard. High resolution mass spectra were obtained on a Bruker APEX IV FT_MS. Elemental analysis was performed on an Elementar Vario EL instrument. UV-vis spectra were recorded on a Shimadzu UV-1601PC spectrophotometer. Fluorescence emission spectra were taken on a Hitachi F-4500 fluorescence spectrophotometer.

EPR spectra were obtained on a Bruker ESP-300E spectrometer at 9.75 GHz, X-band with 100 Hz field modulation, using TEMP as spin trapping agent. Samples were injected quantitatively into home-made quartz capillaries, then illuminated in the cavity of the EPR spectrometer with a Nd:YAG laser at 532 nm (5-6 ns of pulse width, 10 Hz of repetition frequency, 10 mJ/pulse energy).

Time-resolved absorption spectra were measured on a LP-920 laser flash photolysis setup (Edinburgh), using a computer-controlled Nd:YAG laser as the excitation light with an optical absorbance > 0.6 at the excitation wavelength. The laser and

analyzing light beam passed perpendicularly through a 1 cm quartz cell. The complete time-resolved spectra were obtained using a gated CCD camera (Andor iSTAR); the kinetic traces were detected by a Tektronix TDS 3012B oscilloscope and a R928P photomultiplier and analyzed by Edinburgh analytical software (LP920). All samples were deaerated for 20 min with high-purity argon before measurements. All measurements were carried out at room temperature.

$^1O_2$ measurement

The reaction of $^1O_2$ with DPBF (in CH_3CN) or AMDA (in PBS solutions) was adopted to assess the $^1O_2$ generation ability. A series of 2 mL of air-saturated solutions of DPBF or AMDA and the examined complex, of which the absorbance at 500 nm was adjusted to the same, were illuminated with the light of 500 nm (obtained from a Hitachi F-4500 fluorescence spectrophotometer). The consumption of DPBF or AMDA was monitored by absorption bleaching at 405 nm.

DNA electrophoresis

Supercoiled pUC19 plasmid DNA was used as target for studying DNA damage abilities of the examined complexes. 50 μL of supercoiled pUC19 DNA (40 μg/mL) was at first incubated with the examined complexes for 30 min. The mixture was then irradiated with visible light for 40 min, which was obtained from a 1000 W solar simulator (Oriel 91192) using a 470 nm-long pass glass filter and a distilled water pool to cut off the UV and IR light. After irradiation, 20 μL Loading buffer was added. 10 μL of sample was taken for agarose gel electrophoresis (in Tris-acetic acid-EDTA buffer, pH 8.0) at 80 V for 1.5 h. The gel was stained with EB (1 mg/L in H_2O) for 0.5 h and then analyzed using a Gel Doc XR system (Bio-Rad).

MTT assay

All tissue culture media and reagent were purchased from Hy-Clone, Thermo Scientific. The human lung carcinoma cells A549 were grown in DMEM containing 10% fetal bovine serum. Cultures were maintained at 37°C under an appropriate atmosphere with 5% CO_2.

A549 cells were plated at 2×10^5 per well in a Nunc 96 well plate and allowed to grow for 24 h. The cells were exposed to increasing concentrations of the examined complexes and incubated for 4 h, and then irradiated by a solar simulator ($\lambda >$ 400 nm) for 1 h. After another 20 h of incubation, the loading medium was removed and the cells were fed with medium containing MTT from Sigma. Dark controls were run in parallel. Cell survivals were obtained by analysis of the absorbance at 570 nm using a Thermo MK3 Multiscan microplate reader. The data were normalized to 100% viable (untreated) cells.

Acknowledgements

This work was financially supported by the Ministry of Science and Technology (2013CB933801) and NNSFC (21390400, 21172228, 21273259, 21301182, 81171633).

Notes and references

[a] *Key Laboratory of Photochemical Conversion and Optoelectronic Materials, Technical Institute of Physics and Chemistry, Chinese Academy of Sciences, Beijing 100190, P. R. China; E-mail: xswang@mail.ipc.ac.cn and zhouqianxiong@mail.ipc.ac.cn*

[b] *Graduate School of Chinese Academy of Sciences, Beijing 100049, P. R. China.*

† Electronic Supplementary Information (ESI) available: Absorption and emission spectra changes of **1-6** in PBS or CH_3CN in the dark or upon irradiation at $\lambda > 470$ or at 500 nm, ^1H NMR spectra of **1-2** before and after irradiation, EPR signals of **1-6** in CH_3CN in different conditions, AMDA bleaching in the presence of **1-6** in PBS, DNA electrophoresis in the dark, IC_{50} values of **1-6** against A459 cells. See DOI: 10.1039/b000000x/

‡ Footnotes should appear here. These might include comments relevant to but not central to the matter under discussion, limited experimental and spectral data, and crystallographic data.

1 (a) P. Rai, S. Mallidi, X. Zheng, R. Rahmanzadeh, Y. Mir, S. Elrington, A. Khurshid and T. Hasan, *Adv. Drug Delivery Rev.*, 2010, **62**, 1094-1124; (b) J. P. Celli, B. Q. Spring, I. Rizvi, C. L. Evans, K. S. Samkoe, S. Verma, B. W. Pogue and T. Hasan, *Chem. Rev*., 2010, **110**, 2795-2838; (c) D. Crespy, K. Landfester, U. S. Schubert and A. Schiller, *Chem. Commun.*, 2010, **46**, 6651-6662.

2 (a) A. E. O'Connor, W. M. Gallagher and A. T. Byrne, *Photochem. Photobiol.*, 2009, **85**, 1053-1074; (b) M. R. Detty, S. L. Gibson and S. J. Wagner, *J. Med. Chem*., 2004, **47**, 3897-3915.

3 (a) M. C. DeRosa and R. J. Crutchley, *Coord. Chem. Rev*., 2002, **233-234**, 351-371; (b) A. L. Harris, *Nat. Rev. Cancer*, 2002, **2**, 38-47.

4 (a) K. Li, W. H. Lei, G. Y. Jiang, Y. J. Hou, B. W. Zhang, Q. X. Zhou and X. S. Wang, *Langmuir*, 2014, **30**, 14573-14580; (b) J. G. Wang, Y. J. Hou, W. H. Lei, Q. X. Zhou, C. Li, B. W. Zhang and X. S. Wang, *ChemPhysChem*., 2012, **13**, 2739-2747; (c) G. Y. Jiang, W. H. Lei, Q. X. Zhou, Y. J. Hou, X. S. Wang and B. W. Zhang, *Phys. Chem. Chem. Phys*., 2010, **12**, 12229-12236.

5 (a) Y. J. Chen, W. H. Lei, G. Y. Jiang, Q. X. Zhou, Y. J. Hou, C. Li, B. W. Zhang and X. S. Wang, *Dalton Trans*., 2013, **42**, 5924-5931; (b) Y. Sun, Y. Zheng, W. H. Lei, Q. X. Zhou, Y. J. Hou, B. W. Zhang and X. S. Wang, *Dalton Trans*., 2012, **41**, 651-657; (c) Q. X. Zhou, W. H. Lei, J. R. Chen, C. Li, Y. J. Hou, X. S. Wang and B. W. Zhang, *Chem. Eur. J*. 2010, **16**, 3157-3165.

6 (a) N. P. E. Barry and P. J. Sadler, *Chem Commun*., 2013, **49**, 5106-5131; (b) T. Gianferrara, I. Bratsos and E. Alessio, *Dalton Trans*., 2009, 7588-7598.

7 (a) J. Suryadi and U. Bierbach, *Chem. Eur. J*., 2012, **18**, 12926-12934; (b) Ž. D. Bugarčić, J. Bogojeski, B. Petrović, S. Hochreuther and R. Eldik, *Dalton Trans*., 2012, **41**, 12329-12345.

8 (a) Q. X. Zhou, W. H. Lei, Y. J. Hou, Y. J. Chen, C. Li, B. W. Zhang and X. S. Wang, *Dalton Trans*., 2013, **42**, 2786-2791; (b) S. Betanzos-Lara, L. Salassa, A. Habtemariam, O. Novakova, A. M. Pizarro, G. J. Clarkson, B. Liskova, V. Brabec and P. J. Sadler, *Organometallics*, 2012, **31**, 3466-3479; (c) S. Betanzos-Lara, L. Salassa, A. Habtemariam and P. J. Sadler, *Chem. Commun*., 2009, 6622-6624.

9 (a) Z. Li, A. David, B. A. Albani, J.-P. Pellois, C. Turro and K. R. Dunbar, *J. Am. Chem. Soc.*, 2014, **136**, 17058-17070; (b) R. N. Garner, L. E. Joyce and C. Turro, *Inorg. Chem*., 2011, **50**, 4384-4391; (c) R. N. Garner, J. C. Gallucci, K. R. Dunbar and C. Turro, *Inorg. Chem*., 2011, **50**, 9213-9215.

10 (a) A. N. Hidayatullah, E. Wachter, D. K. Heidary, S. Parkin and E. C. Glazer, *Inorg. Chem.,* 2014, **53**, 10030-10032; (b) E. Wachter, B. S. Howerton, E. C. Hall, S. Parkin and E. C. Glazer, *Chem. Commun.,* 2014, **50**, 311-313; (c) B. S. Howerton, D. K. Heidary and E. C. Glazer, *J. Am. Chem. Soc*., 2012, **134**, 8324-8327.

11 (a) F. Schmitt, N. P. E. Barry, L. Juillerat-Jeanneret and B. Therrien, Bioorg. *Med. Chem. Lett*., 2012, **22**, 178-180; (b) P. Sweigert, Z. Xu, Y. Hong and S. Swavey, *Dalton Trans.*, 2012, **41**, 5201-5208; (c) Z. Xu and S. Swavey, *Dalton Trans*., 2011, **40**, 7319-7326; (d) T. Gianferrara, A. Bergamo, I. Bratsos, B. Milani, C. Spagnul, G. Sava and E. Alessio, J. Med. Chem., 2010, **53**, 4678-4690; (e) T. Gianferrara, I. Bratsos, E. Iengo, B. Milani, A. Oštrić, C. Spagnul, E. Zangrando and E. Alessio, *Dalton Trans*., 2009, 10742-10756; (f) F. Schmitt, P. Govindaswamy, G. Süss-Fink, W. H. Ang, P. J.

Dyson, L. Juillerat-Jeanneret and B. Therrien, *J. Med. Chem*., 2008, **51**, 1811-1816.

12 (a) C. Mari, V. Pierroz, R. Rubbiani, M. Patra, J. Hess, B. Spingler, L. Oehninger, J. Schur, I. Ott, L. Salassa, S. Ferrari and G. Gasser, *Chem. Eur. J*., 2014, **20**, 14421-14436; (b) R. Lincoln, L. Kohler, S. Monro, H. Yin, M. Stephenson, R. Zong, A. Chouai, C. Dorsey, R. Hennigar, R. P. Thummel and S. A. McFarland, *J. Am. Chem. Soc*., 2013, **135**, 17161-17175; (c) Y. Liu, R. Hammitt, D. A. Lutterman, R. P. Thummel and C. Turro, *Inorg. Chem*., 2009, **48,** 375-385.

13 (a) J. Wang, J. Newman Jr., S. L. H. Higgins, K. M. Brewer, B. S. J. Winkel and K. J. Brewer, *Angew. Chem., Int. Ed*., 2013, **52**, 1262-1265; (b) S. L. H. Higgins, A. J. Tucker, B. S. J. Winkel and K. J. Brewer, *Chem. Commun*., 2012, **48**, 67-79.

14 Y. J. Chen, W. H. Lei, G. Y. Jiang, Y. J. Hou, C. Li, B. W. Zhang, Q. X. Zhou and X. S. Wang, *Dalton Trans*., 2014, **43**, 15375-15384.

15 B. A. Albani, B. Peña, N. A. Leed, N. A. B. G. de Paula, C. Pavani, M. S. Baptista, K. R. Dunbar and C. Turro, *J. Am. Chem. Soc*., 2014, **136**, 17095-17101.

16 Q. X. Zhou, F. Yang, W. H. Lei, J. R. Chen, C. Li, Y. J. Hou, X. C. Ai, J. P. Zhang, X. S. Wang and B. W. Zhang, *J. Phys. Chem*., 2009, **113**, 11521-11526.

17 Q. X. Zhou, W. H. Lei, Y. J. Chen, C. Li, Y. J. Hou, B. W. Zhang and X. S. Wang, *Chem. Eur. J*., 2012, **18**, 8617-8621.

18 (a) C. Hadjur, A. Jeunet and P. Jardon, *J. Photochem. Photobiol.*, B, 1994, **26**, 67-74; (b) Y. Lion, M. Delmelle and A. Van De Vorst, *Nature*, 1976, **263**, 442-443.

19 R. H. Young, K. Wehrly and R. L. Martin, *J. Am. Chem. Soc.*, 1971, **93**, 5774-5779.

20 A. A. Abdel-Shafi, P. D. Beer, R. J. Mortimer and F. Wilkinson, *J. Phys. Chem. A,* 2000, **104**, 192-202.

21 H. A. Goodwin and F. Lions, *J. Am. Chem. Soc*., 1959, **81**, 6415-6422.

Table of Contents

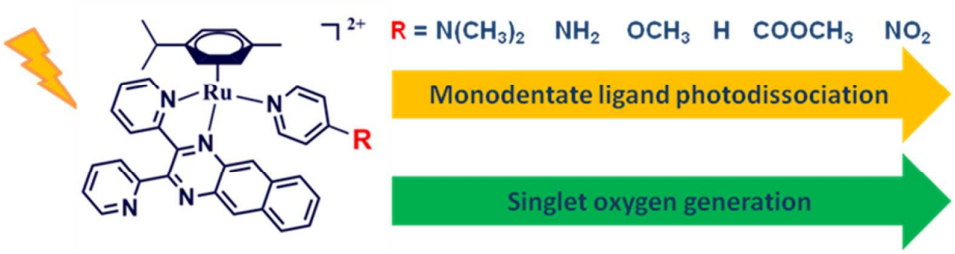

With the increase of the electron-withdrawing strength of the R group, both ligand photodissociation and $^1O_2$ generation of the complexes improved markedly.